



Platinum–tin bimetallic nanoparticles for methanol tolerant oxygen-reduction activity

C. Jeyabharathi^a, P. Venkateshkumar^b, J. Mathiyarasu^{a,*}, K.L.N. Phani^a

^a *Electrodes and Electrocatalysis Division, Central Electrochemical Research Institute, Karaikudi 630006, Tamilnadu, India*

^b *Centre for Education, Central Electrochemical Research Institute, Karaikudi 630006, Tamilnadu, India*

ARTICLE INFO

Article history:

Received 1 May 2008

Received in revised form 20 July 2008

Accepted 22 July 2008

Available online 31 July 2008

Keywords:

Methanol tolerant

Electrocatalysis

Cathode catalyst

Platinum–tin

Oxygen-reduction

ABSTRACT

Carbon-supported Pt–Sn/C bimetallic nanoparticle electrocatalysts were prepared by the simple reduction of the metal precursors using ethylene glycol. The catalysts heat-treated under argon atmosphere to improve alloying of platinum with tin. As-prepared Pt–Sn bimetallic nanoparticles exhibit a single-phase fcc structure of Pt and heat-treatment leading to fcc Pt₇₅Sn₂₅ phase and hexagonal alloy structure of the Pt₅₀Sn₅₀ phase. Transmission electron microscopy image of the as-prepared Pt–Sn/C catalyst reveals a mean particle diameter of ca. 5.8 nm with a relatively narrow size distribution and the particle size increased to ca. 20 nm when heat-treated at 500 °C due to agglomeration. The electrocatalytic activity of oxygen reduction assessed using rotating ring disk electrode technique (hydrodynamic voltammetry) indicated the order of electrocatalytic activity to be: Pt–Sn/C (as-prepared) > Pt–Sn/C (250 °C) > Pt–Sn/C (500 °C) > Pt–Sn/C (600 °C) > Pt–Sn/C (800 °C). Kinetic analysis reveals that the oxygen reduction reaction on Pt–Sn/C catalysts follows a four-electron process leading to water. Moreover, the Pt–Sn/C catalyst exhibited much higher methanol tolerance during the oxygen reduction reaction than the Pt/C catalyst, assessing that the present Pt–Sn/C bimetallic catalyst may function as a methanol-tolerant cathode catalyst in a direct methanol fuel cell.

© 2008 Elsevier Ltd. All rights reserved.

1. Introduction

There has been a continuing interest in the development of direct methanol fuel cells (DMFC) that find appealing applications in portable devices such as cellular phones, laptops, etc. Despite the progress, its performance is still limited because of poor kinetics of the anode reaction, poisoning of catalyst material [1] and methanol cross-over from anode to cathode through the polymer electrolyte membrane [2]. To cope with the methanol cross-over problem, several methanol tolerant cathode catalysts such as chevral phase type compounds [3,4], N₄ macrocyclic complexes [5–7], binary platinum alloys [8–12] where the secondary elements are Ni, Cr, Co, Fe, and Bi, binary palladium alloys [13,14] and ternary alloys [15] have been employed. Although the reported catalysts show high methanol tolerance, a “trade-off” between the oxygen reduction reaction (ORR) activity and methanol tolerance and the stability of these catalysts under fuel cell conditions still has to be improved. Hence there is great concern in the development of selective cathode catalysts with selectivity to oxygen reduction reaction especially in the presence of methanol, to harvest better efficiency in DMFCs.

Zinola et al. [16] reported that Sn underpotential deposit on Pt to be a catalyst for oxygen reduction to bulk hydrogen peroxide and water. Though some studies report that Sn enhances the catalytic activity of Pt towards methanol oxidation [17–19], there are reports of low or no enhancement of methanol oxidation by Sn when Pt–Sn alloy systems are used [20–22]. In fact, such enhancements were later found to be due to other overriding factors than the effect of Sn on methanol oxidation, typically involving “ensemble” effects [23]. Pt–Sn catalysts have also been employed for carbon monoxide oxidation [25–28], ethanol oxidation [29–33], hydrogenation reaction [34–36] and dehydrogenation of isobutene [37]. Colmati et al. [24] reported that adsorption/dehydrogenation of methanol becomes more difficult due to alloying of Sn with Pt and methanol oxidation occurs only at moderate alloying. Hence, it is of interest to examine if Pt–Sn alloy system could be a methanol tolerant cathode catalyst (for oxygen reduction) in DMFC. It is intriguing to find that Pt–Sn/C system has not been reported thus far in the case of oxygen reduction reaction, to our knowledge. Preliminary studies on its ORR activity were recently carried out in our laboratories [38]. During these investigations, we observed this mixed behaviour of Pt–Sn/C wherein the as-prepared catalyst is different from those subjected to heat-treatment. In what follows, we show that on heat-treatment, methanol oxidation activity of the catalyst decreases whereas the ORR activity is retained in tact. Alloying is

* Corresponding author.

E-mail address: al.mathi@yahoo.com (J. Mathiyarasu).

expected to bring in changes in the Pt–Pt distance that dictates the course of oxygen reduction. In what follows, we show that alloy formation and the heat-treatment of the catalysts have significant influence on the ORR activity and inhibition of methanol oxidation.

We synthesized carbon-supported Pt–Sn catalyst by simple polyol reduction process and used as a catalyst for ORR. The effects of heat-treatment of catalyst under argon atmosphere were studied towards oxygen reduction reaction in presence of methanol, besides the kinetics of ORR on these catalyst materials.

2. Experimental

2.1. Materials

All chemicals used were of analytical grade. $\text{H}_2\text{PtCl}_6 \cdot 6\text{H}_2\text{O}$, GR (Merck) and $\text{SnCl}_2 \cdot 2\text{H}_2\text{O}$, GR (Merck) were used as metal precursors. Vulcan XC72R was used for supporting the metal nanoparticles. Ethylene glycol, GR (Merck) was used as a solvent and reducing agent. All the solutions were prepared with ultra-pure water (MilliQ, Millipore).

2.2. Synthesis of carbon supported Pt–Sn

Pt–Sn (70%:30%)/C nanoparticle samples were prepared by a polyol reduction process. In this process, to a mixture of 9.28 mg of $\text{H}_2\text{PtCl}_6 \cdot 6\text{H}_2\text{O}$, 28.51 mg of $\text{SnCl}_2 \cdot 2\text{H}_2\text{O}$ and 125 mg of Vulcan XC72R carbon, 40 mL of ethylene glycol was added and stirred well to obtain a homogeneous mixture. This was refluxed at 85 °C for 4 h and was kept aside to cool at room temperature and the black residue was centrifuged, washed three times with Millipore water ($18.2 \text{ M}\Omega \text{ cm}^{-1}$), followed by acetone wash. The residue was kept under vacuum for drying at room temperature. The carbon-supported metal nanoparticles were subjected to heat-treatment in argon atmosphere at various temperatures, viz., 250, 500, 600 and 800 °C separately for 4 h in a tubular furnace.

2.3. X-ray diffraction

X-ray diffraction (XRD) measurements of Pt–Sn/C catalysts were carried out on a Philips PANalytical X-ray diffractometer using Cu K α radiation ($\lambda = 0.15406 \text{ nm}$). The XRD spectra were obtained using high resolution in the step-scanning mode with a narrow receiving slit (0.5°) with a counting time of 15 s per 0.1°. Scans were recorded in the 2θ range of 15–90°. The identification of the phases was made by referring to the Joint Committee on Powder diffraction Standards International Center for Diffraction Data (JCPDS-ICDD) database.

2.4. Transmission electron microscopy

Transmission electron microscopic (TEM) analysis was performed using TEM microscope JEOL, JEM 3010, URP, operating at 300 kV and having a resolution of 0.17 nm. The samples for the TEM characterization were prepared as follows: a carbon film was deposited onto a mica sheet that was placed onto the Cu grids (300 mesh and 3 mm diameter). The material to be examined was dispersed in water by sonication, placed onto the carbon film and left to dry. The average particle size was calculated using about 300 particles.

2.5. Electrochemical characterization

The performance of Pt–Sn/C catalysts in comparison with commercial Pt/C (40 wt.%, E-Tek) catalyst for the ORR was evaluated

primarily with a half-cell configuration based on the linear scan voltammogram (LSV) measurements. Ten milligrams of catalysts, 0.5 mL of Nafion solution (5 wt.%, Aldrich) and 2.5 mL of water were mixed ultrasonically. A measured volume (3 or 10 μL) of this ink was transferred via a syringe onto a freshly polished glassy carbon disk (3 or 6 mm in diameter). After the solvents were evaporated overnight at room temperature, the prepared electrode served as the working electrode.

Electrochemical measurements were performed using a BAS 100B or Autolab PGSTAT 30 potentiostat/galvanostat (for RRDE experiments where the equipment is coupled BIPOT module) and a conventional three-electrode electrochemical cell. The counter electrode was a platinum foil and a mercury/mercurous sulfate electrode served as the reference electrode. However, all potentials are referred to the normal hydrogen electrode (NHE). The electrolyte used for half-cell measurements was 0.5 M $\text{H}_2\text{SO}_4 + 0.5 \text{ M CH}_3\text{OH}$. Due to a slight contamination from the Nafion solution, the porous electrodes were cycled at a scan rate of 50 mV s^{-1} between 0.03 and 1.18 V vs. NHE until reproducible cyclic voltammograms were obtained, prior to any LSV measurements. The electrochemical activity for the ORR was measured with the rotating ring disk electrode (RRDE) technique using an interchangeable ring-disk electrode setup coupled with a rotation controller (Pine Instruments). 6 mm o.d. \times 4 mm thick interchangeable glassy carbon served as a disc electrode and 0.5 mm fixed platinum ring (99.99% Pt, 6.5 mm i.d., 7.5 mm o.d.) separated by a thin Teflon spacer as ring electrode. 10 μL of the catalyst ink was placed precisely over the disc electrode without spreading over ring electrode for each experiment. High purity nitrogen and oxygen were used for deaeration and oxygenation of the solutions, respectively. During the measurements, a blanket of nitrogen or oxygen was maintained above the electrolyte surface. Unless stated otherwise, all half-cell tests were performed at a temperature of $25 \pm 1^\circ\text{C}$.

3. Results and discussions

3.1. Characterization of Pt–Sn/C

Fig. 1 shows the powder XRD patterns of Pt–Sn/C catalysts. All the reflections of the as-prepared Pt–Sn/C, Pt–Sn/C (250 °C) and Pt–Sn/C (500 °C) show the *fcc* structure of crystalline Pt. But the 2θ value shifts to lower values indicating alloying of Pt with Sn, since Sn enters *fcc* lattice of Pt. For the as-prepared Pt–Sn/C sample, there are low intensity peaks at $\sim 33^\circ$ and $\sim 52^\circ$ corresponding to (101) and (211) planes of tetragonal structure of SnO_2 . The XRD patterns of Pt–Sn/C samples heat-treated at 600 and 800 °C clearly show the formation of stoichiometric cubic $\text{Pt}_{75}\text{Sn}_{25}$ alloy phase along with secondary phase, i.e., hexagonal $\text{Pt}_{50}\text{Sn}_{50}$ alloy formation. The intensity and sharpness of the peak and the lattice parameter increasing with temperature of heat-treatment, all point to an increase in the Pt–Pt distance. As can be seen from the TEM images, the heat-treatment causes particle agglomeration, thus leading to increase in the particle size.

Fig. 2 shows the TEM images of the heat-treated Pt–Sn/C catalyst materials. The as-prepared Pt–Sn/C shows a mean particle diameter of ca. 5.8 nm. The nanoparticles are well dispersed on the surface of the support with a relatively narrow particle size distribution. Heat-treatment leads to the particle agglomeration and the particle size increases to ca. 20 nm at 500 °C. The particle size calculated from XRD using Scherrer's formula is in fairly good agreement with the average particle size calculated using TEM measurements (Table 1).

Fig. 3 shows the cyclic voltammograms of Pt–Sn/C catalysts in a solution of 0.5 M sulfuric acid at a scan rate of 100 mV s^{-1} and in a

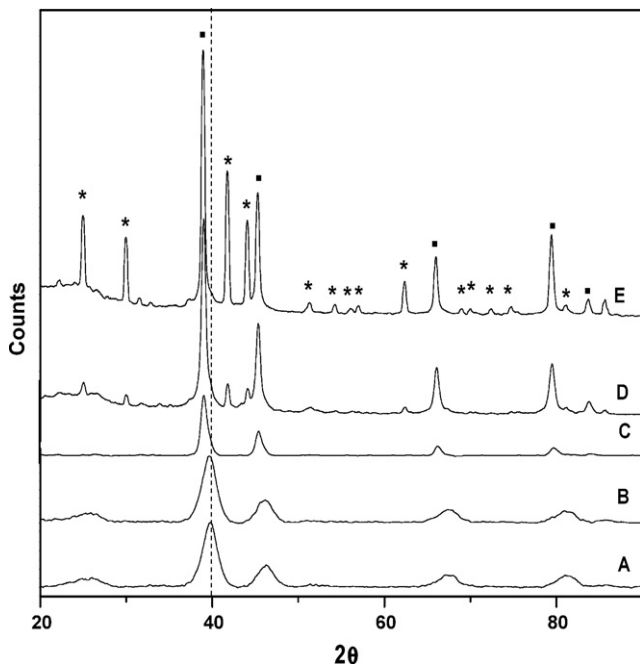


Fig. 1. XRD patterns of (A) Pt–Sn/C (as-prepared), (B) Pt–Sn/C (250°C), (C) Pt–Sn/C (500°C), (D) Pt–Sn/C (600°C) and (E) Pt–Sn/C (800°C); (*) reflections for hexagonal $\text{Pt}_{50}\text{Sn}_{50}$ phase; (■) reflections for cubic $\text{Pt}_{75}\text{Sn}_{25}$ phase.

potential range of 0.03 to 1.33 V (NHE). With as-prepared Pt–Sn/C, surface oxidation of Sn starts at ~ 0.2 V more negative than the onset of surface oxidation of Pt/C (see Fig. 3), according to that reported in Ref. [39]. The peak potential of Sn oxidation is centered at ~ 0.75 V. Single reduction peak during the cathodic scan observed with all the catalysts corresponds to the reduction of both Pt oxide and Sn in higher oxidation states. It could be clearly seen from the voltammogram that the stripping current decreases with the heat-treatment, which shows that Sn is alloyed with Pt and the degree of alloying increases with temperature. It is important to note that the extent of Sn dissolution (centering on 0.7 V) decreases and hence the stability of the catalyst improves with heat-treatment. It is also obvious from the CV's that hydrogen adsorption–desorption current decreases as the temperature of heat-treatment of catalyst increases. Incorporation of Sn appears to block the Pt active sites affecting the hydrogen adsorption–desorption properties of Pt–Sn/C catalysts contrary to Pt/C [29,40].

Fig. 4 shows the cyclic voltammetry of methanol oxidation on Pt–Sn/C catalysts in comparison with that of Pt/C 40% (E-TEK) in solutions of 0.5 M sulfuric acid + 0.5 M methanol. Methanol oxidation current on the as-prepared Pt–Sn/C catalyst is 25% less than that of Pt/C. It is interesting that methanol oxidation current decreases drastically as the temperature of heat-treatment of Pt–Sn/C catalyst increases. This shows that the degree of alloying of Sn with Pt increases as the temperature of heat-treatment increases. As a consequence, the number of Pt active site decrease that causes a reduction in the methanol oxidation current.

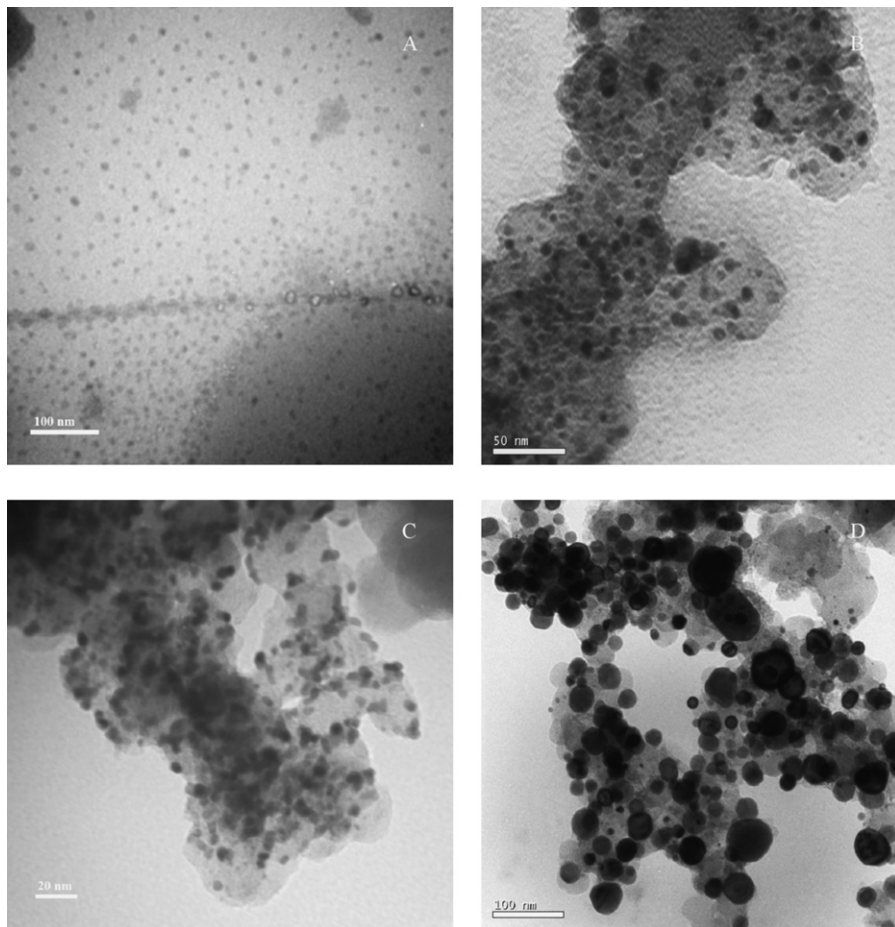


Fig. 2. TEM images of (A) Pt–Sn/C as-prepared, (B) Pt–Sn/C (250°C), (C) Pt–Sn/C (500°C) and (D) Pt–Sn/C (800°C).

Table 1

Values of Lattice parameter and particle size for Pt–Sn/C catalysts

Catalyst	Pt ₇₅ Sn ₂₅ phase	Pt ₅₀ Sn ₅₀ phase	Particle size (nm)	
	Lattice parameter (nm)	Lattice parameter (nm)	XRD	TEM
Pt–Sn/C (as-prepared)	$a_0 = 0.3929$	—	5.79	6 ± 0.6
Pt–Sn/C (250 °C)	$a_0 = 0.3931$	—	5.63	5 ± 0.7
Pt–Sn/C (500 °C)	$a_0 = 0.3997$	—	16.68	6 ± 0.9
Pt–Sn/C (600 °C)	$a_0 = 0.4000$	$a_0 = 0.4130 c_0 = 0.5446$	20.73	—
Pt–Sn/C (800 °C)	$a_0 = 0.4000$	$a_0 = 0.4130 c_0 = 0.5446$	26.97	25 ± 0.5

Lattice parameter of Pt = 0.3923 nm.

Table 2

Parameters derived from hydrodynamic polarization curves of ORR

Catalyst	Half wave potential at 1600 rpm (mV) (data collected from Fig. 5)	ORR current density (mA cm^{-2}) (at 0.55 V)	B value ^a , $\text{mA}/\text{rpm}^{0.5}$ (from hydrodynamic voltammetry)	Tafel slope (mV dec ⁻¹) (± 2)	% H_2O_2 calculated
Pt/C	780	2.74	0.128	118	0.76
Pt–Sn/C (as-prepared)	765	2.87	0.129	120	2.14
Pt–Sn/C (250 °C)	730	2.77	0.127	130	1.84
Pt–Sn/C (500 °C)	725	2.68	0.117	120	1.38
Pt–Sn/C (600 °C)	680	2.32	0.116	120	2.48
Pt–Sn/C (800 °C)	650	2.04	0.105	120	2.30

^a Value calculated for 4e transfer is: 0.130 mA/rpm^{0.5}.

3.2. ORR activity and methanol tolerance of Pt–Sn/C catalysts

To study the electrocatalytic activity and kinetics of oxygen reduction reaction on the heat-treated Pt–Sn/C catalysts, RDE experiments were performed with different rotation rates in 0.5 M sulfuric acid saturated with oxygen in the oxygen reduction potential region, i.e., from 0.1 to 1 V at a scan rate of 5 mV s⁻¹. In Fig. 5, a comparison of the polarization curves obtained for ORR on Pt–Sn/C catalysts with those on Pt/C at a rotation rate of 1600 rpm. From the half wave potentials (Table 2), it can be noted that the ORR activity of the as-prepared Pt–Sn/C catalyst is comparable to that of Pt/C and the order of electrocatalytic activity towards ORR is

Pt–Sn/C(as-prepared) > Pt–Sn/C(250 °C) > Pt–Sn/C(500 °C)

> Pt–Sn/C(600 °C) > Pt–Sn/C(800 °C)

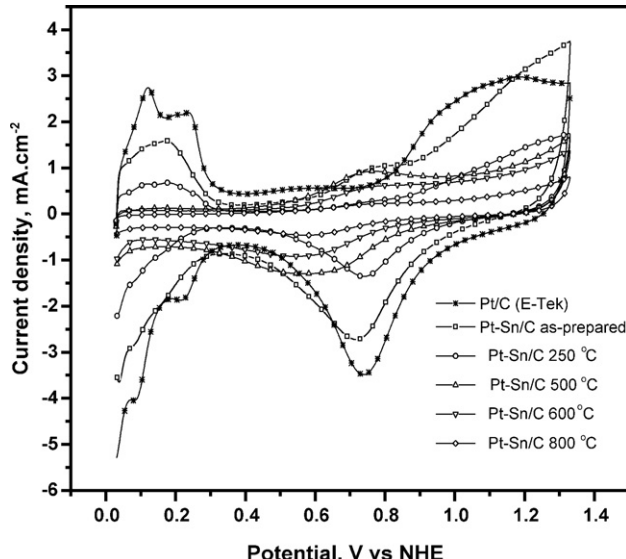


Fig. 3. Cyclic voltammograms obtained on a Pt–Sn/C electrode surfaces and compared with that of Pt40 % (E-Tek) in 0.5 M H_2SO_4 solution; sweep rate 100 mV/s.

But there is no significant change in the current density of ORR in all the cases. A slight decrease in the ORR current on heat-treatment may be attributed to a possible change in the surface structure of the catalyst. By far, the polarization behaviour of Pt–Sn/C (500 °C) is closest to that of Pt/C, though associated with a cathodic shift of half-wave potential by about ~60 mV. It is conjectured that the surface structure will play a greater role than that is assessed through XRD in this work. However, the present studies are a possible pointer to the general characteristics of Pt–Sn/C for the reactions of oxygen reduction and methanol oxidation.

Fig. 6 presents a comparison of the polarization curves of ORR on Pt–Sn/C catalysts with that of Pt/C in 0.5 M sulfuric acid containing 0.5 M methanol obtained at a rotation rate of 1600 rpm. For Pt/C, there is a significant increase in the over potential of ORR

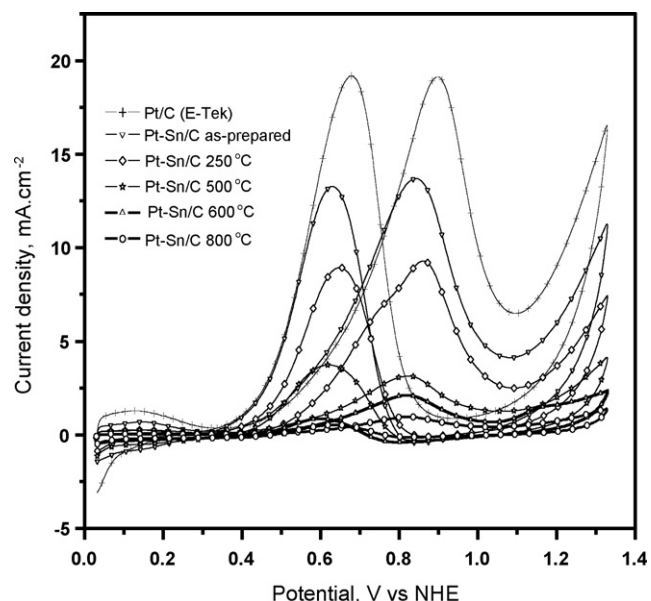


Fig. 4. Cyclic voltammograms of methanol oxidation obtained on a Pt–Sn/C electrode surfaces and compared with that of Pt40 % (E-Tek) in 0.5 M H_2SO_4 solution containing 0.5 M methanol; sweep rate 100 mV/s.

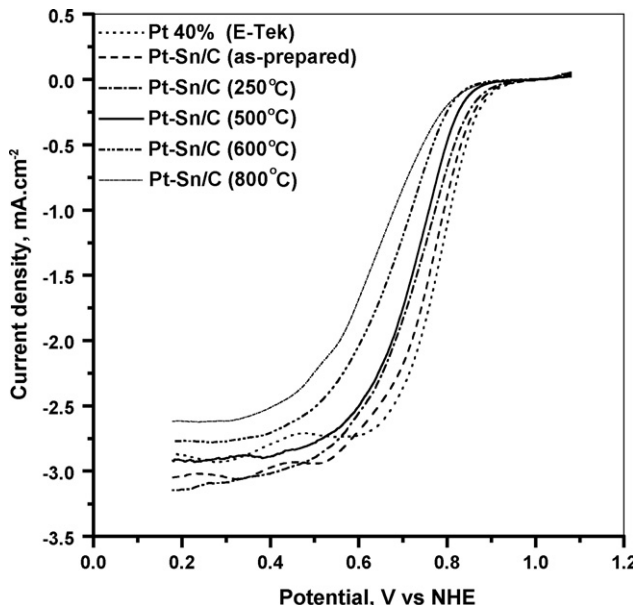


Fig. 5. Polarization curves obtained with a RDE for O₂ reduction on a Pt–Sn/C electrode surfaces and compared with Pt40 % (E-Tek) in 0.5 M H₂SO₄ solution at 1600 rpm; sweep rate 5 mV/s.

which is obviously due to the simultaneous oxidation of methanol and oxygen reduction. The half-wave potential of oxygen reduction on Pt–Sn/C catalysts in the presence of methanol shifts in the anodic direction as the temperature of heat-treatment increases (half wave potentials are: 580, 570, 605, 630, 625 and 625 mV on Pt/C, Pt–Sn/C (as-prepared), Pt–Sn/C (250 °C), Pt–Sn/C (500 °C), Pt–Sn/C (600 °C) and Pt–Sn/C (800 °C), respectively). For Pt–Sn/C (800 °C), the methanol oxidation current is completely absent. The half-wave potential of oxygen reduction on Pt–Sn/C (800 °C) catalyst in the presence of methanol shifts cathodically by 25 mV with reference to the solution conditions without methanol. Considering the gain in terms of methanol tolerant character of the catalyst,

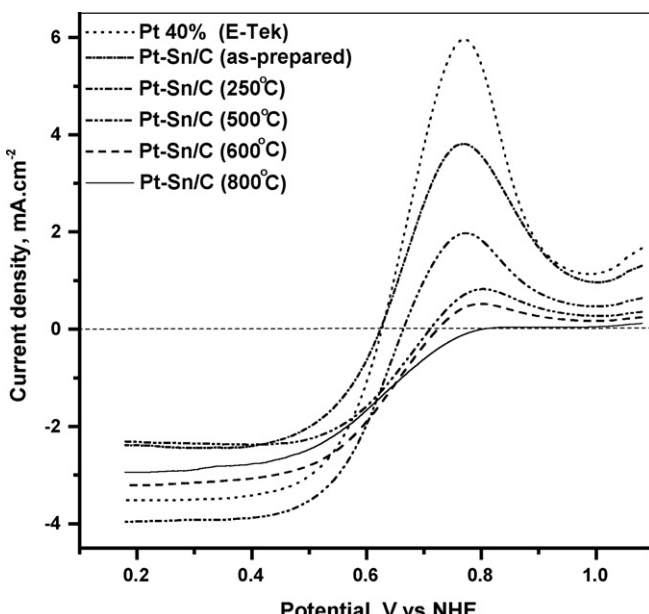


Fig. 6. Polarization curves obtained with a RDE for O₂ reduction on a Pt–Sn/C electrode surfaces and compared with Pt40% (E-Tek) in 0.5 M H₂SO₄ solution containing 0.5 M methanol at 1600 rpm; sweep rate 5 mV/s.

a cathodic shift of 25 mV can be a *trade-off* [29,40,9,14]. This is too less when compared with the corresponding shift >200 mV for Pt/C. This small shift suggests that there is always a “*trade-off*” between methanol oxidation and oxygen reduction, as has been observed in Refs. [9,14,41,42].

The catalytic current density, *i* and kinetic current density, *i_k* are related by the Koutecky–Levich equation [43],

$$\frac{1}{i} = \frac{1}{i_k} + \frac{1}{i_d} = \frac{1}{i_k} + \frac{1}{0.2nFD_0^{2/3}\omega^{1/2}\nu^{-1/6}C_0} = \frac{1}{i_k} + \frac{1}{B\omega^{1/2}}$$

where *i_k* is the kinetic current density, *B* is the Levich slope, ‘*n*’ the number of electrons involved in the ORR per oxygen molecule, ‘*C*’ the saturation concentration for oxygen in the electrolyte (1.26×10^{-3} mol/L), ‘*D*’ is the diffusion coefficient (1.93×10^{-5} cm²/s), ‘*v*’ the kinematic viscosity of the solution (1.009×10^{-2} cm²/s) and ‘*ω*’ is the rotation rate in rpm. The number of electrons involved in the ORR was calculated using the Koutecky–Levich equation, which relates the current density *i* to the rotation rate of the electrode, *ω*. A plot of *i*⁻¹ vs. *ω*^{-1/2} should give parallel straight lines for different potentials in mixed kinetic-diffusion controlled region. The K–L plot of all Pt–Sn/C catalysts shows the linearity and parallelism, confirming that oxygen reduction reaction follows first order kinetics with respect to molecular oxygen. The number of electrons calculated using slope of K–L plot is given in the Table 2. From the number of electrons calculated, it can state that oxygen reduction on Pt–Sn/C catalysts occurs through a direct reduction of oxygen to water. The percentage of hydrogen peroxide generated at the ring at 0.4 V is calculated using the equation,

$$\%H_2O_2 = \frac{2I_R/N}{I_D + (I_R/N)}$$

where *I_D* and *I_R* are the disc and ring currents, respectively and *N* is the collection efficiency (0.24). The percentage of peroxide calculated for Pt–Sn/C catalysts is not significant even in the potential region where hydrogen peroxide formation is expected to be very high and is listed in the Table 2. The kinetic current density *i_k* can be obtained by extrapolating the K–L plots for *ω*^{-1/2} → 0. From the kinetic current density, the Tafel slope values are calculated by plotting log *i_k* vs. potential obtained in the mixed kinetic-diffusion controlled region is given in Table 2. The Tafel slope value determined to be 120 mV dec⁻¹ suggests that the first electron transfer is the rate-determining step. The Tafel slope calculated for Pt–Sn/C catalyst is also 120 mV dec⁻¹ suggesting that ORR mechanism is similar to that of Pt/C. This is sufficient proof to say that the mechanism of ORR does not change with the introduction of Sn into Pt, based on the observations: (i) a Tafel slope of ~120 mV dec⁻¹; (ii) approximately 2.5% of peroxide formation found in this work is much less than the values reported in the recent literature, for example, Pd–Fe/C wherein the extent of peroxide formation reported is around 4.1% [14], suggesting that a direct 4e-pathway is possibly occurring on Pt–Sn/C surface. It is now certain that peroxide formation is also a factor to be considered in the case of Pt–Sn/C catalysts for oxygen reduction. Considering these factors, Pt–Sn/C (250 °C) or Pt–Sn/C (500 °C) appear to be optimally placed with regard to the well-defined polarization behaviour and lower extent of peroxide formation, though associated with a cathodic shift of the half-wave potential. It is probable that as the heat-treatment temperature increases, surface enrichment of Sn may also take place that can affect the geometry needed for ORR to occur. However, it is difficult to comment on the dependence of the extent of peroxide formation on the treatment conditions.

It is well known that the crossover of methanol from the anode compartment to the Pt cathode leads to a competitive reaction

between oxygen reduction and methanol oxidation. The Pt sites are occupied by CO_{ads} which reduces the overall cell voltage [44,45]. Thus, it is highly desirable to develop selective-ORR electrocatalysts that have a high methanol tolerance for DMFC applications. The structure and composition of the catalysts are two key points in determining the adsorption/catalytic properties. Mainly, the activity enhancement in the ORR on platinum based alloy catalysts could be correlated to the changes in structural parameters [2]. The alloying of Pt–Sn/C catalyst improves upon heat-treatment and there is a clear transformation of Pt *fcc* phase to a stoichiometric *fcc* $\text{Pt}_{75}\text{Sn}_{25}$ and secondary hexagonal $\text{Pt}_{50}\text{Sn}_{50}$ phase. The lattice parameter for *fcc* phase of Pt is 0.3923 nm whereas for the Pt–Sn catalysts, it increases from 0.3923 nm to higher values due to the miscibility of Sn in Pt network. It can be expected that as the lattice parameter increases the Pt–Pt distance also increases. This result is contrary to the Pt–M system (M = first transition elements), where the lattice parameter is reported decreasing [20]. Being a p-block element, the size of the Sn atom is expected to be more compared to the transition metal and hence increase Pt–Pt distance. It is also likely that Sn may be introduced in the Pt phase as its oxide. However, it is difficult to comment on the exact mechanism for the increase in the lattice parameter without more rigorous structural analysis. Clearly methanol oxidation on Pt–Sn/C current decreases as the Pt–Pt distance in Pt–Sn/C increases upon heat-treatment. It is well known that this increased Pt–Pt distance is unfavorable to methanol adsorption that requires a minimum of three Pt sites nearby [46]. But for oxygen adsorption, the required Pt sites are two [47]. The degree of alloying appears to favor minimal adsorption of methanol and thus make the catalyst methanol tolerant. In the presence of methanol, the half-wave potential of methanol oxidation shifts anodically upon heat-treatment. Pt–Sn/C 800 °C shows greater methanol tolerance and the methanol oxidation current is very low at a high concentration of methanol (0.5 M). Kinetics of oxygen reduction observed for Pt–Sn/C remains the same as Pt/C evidenced from the Tafel slope value of ~120 mV dec⁻¹. The linearity and parallelism of the KL plot show that oxygen reduction follows first-order kinetics with respect to molecular oxygen. Therefore, the heat-treatment of the alloy catalyst leads to a structural change which in turn renders the catalyst methanol tolerant and the present Pt–Sn/C bimetallic catalyst is expected to function as a methanol-tolerant cathode catalyst in a direct methanol fuel cell. While the inhibition of methanol oxidation can be satisfactorily explained using the increased Pt–Pt distance in Pt–M alloys, the same argument cannot hold good in the case of the retention of ORR activity. It is likely that local surface structure in contact with the electrolyte solution being the deciding factor can undergo changes that can be sensed only using *in situ* surface analytical techniques. A detailed surface analysis will be able to reveal the real nature of the surface responsible for a balance between ORR activity and methanol tolerance.

4. Conclusions

Pt–Sn/C catalyst is synthesized by polyol reduction process. The size of the particles obtained is very small but the size slightly increases with temperature of heat-treatment. TEM image shows that particles are well distributed on carbon matrix. 2θ values shifted to lower angle in XRD confirm the alloying of Sn with Pt and as the temperature of heat-treatment increases. Lattice parameter value of Pt–Sn/C catalysts increases from that of Pt ($a_0 = 0.3923$ nm) indicating the increasing Pt–Pt distance on increasing heat-treatment. The increased Pt–Pt bond distance creates unfavorable situation for adsorption/dehydrogenation of methanol. Cyclic voltammograms for methanol oxidation show a decrease in methanol oxidation current, as the temperature

of heat-treatment has increased since the degree of alloying increases upon heat-treatment. However, oxygen reduction activity is retained for all the catalysts. The order of oxygen reduction activity is Pt–Sn/C (as-prepared) > Pt–Sn/C (250 °C) > Pt–Sn/C (500 °C) > Pt–Sn/C (600 °C) > Pt–Sn/C (800 °C). The K–L plot of all Pt–Sn/C catalysts shows the linearity and parallelism that confirms that oxygen reduction reaction follow first-order kinetics with respect to molecular oxygen. The Tafel slope calculated for Pt–Sn/C catalyst is ~120 mV dec⁻¹. This suggests that the ORR mechanism is similar to that of Pt/C. The percentage of peroxide calculated for Pt–Sn/C catalysts is negligible even in the potential region where hydrogen peroxide formation is expected to be very high. Thus, oxygen reduction by Pt–Sn/C catalysts occurs through a direct formation of water with a low extent of hydrogen peroxide formation. Thus, Pt–Sn/C alloy catalyst may be a potential candidate even in the presence of methanol.

Acknowledgments

The authors thank the Department of Science & Technology, New Delhi for financial assistance [SR/S1/PC-37/2004] and Professor A.K. Shukla, Director, CECRI for his encouragement.

References

- [1] J.J. Baschuk, X. Li, Int. J. Energy Res. 25 (2001) 695.
- [2] A.S. Arico, S. Srinivasan, V. Antonucci, Fuel Cells 1 (2001) 133.
- [3] N. Alonso-Vante, W. Jaegermann, H. Tributsch, W. Honle, K. Yvon, J. Am. Chem. Soc. 109 (1987) 3251.
- [4] O. Solorza-Feria, K. Ellmer, M. Giersig, N. Alonso-Vante, Electrochim. Acta 39 (1994) 1647.
- [5] K. Wiesener, D. Ohms, V. Neumann, R. Franke, Mater. Chem. Phys. 22 (1989) 457.
- [6] G.Q. Sun, J.T. Wang, R.F. Savinell, J. Appl. Electrochem. 28 (1998) 1087.
- [7] S. Gupta, D. Tryk, S.K. Zecevic, W. Aldred, D. Guo, R.F. Savinell, J. Appl. Electrochem. 28 (1998) 673.
- [8] T. Toda, H. Igarashi, M. Watanabe, J. Electroanal. Chem. 460 (1999) 258.
- [9] H. Yang, N. Alonso-Vante, J.-M. Leger, C. Lamy, J. Phys. Chem. B 108 (2004) 1938.
- [10] E. Antolini, J.R.C. Salgado, E.R. Gonzalez, Appl. Catal. B: Environ. 63 (2005) 137.
- [11] A.V. Ye Xu, M. Ruban, Mavrikakis, J. Am. Chem. Soc. 126 (2004) 4717.
- [12] A.K. Shukla, R.K. Raman, N.A. Choudhury, K.R. Priolkar, P.R. Sarode, S. Emura, R. Kumashiro, J. Electroanal. Chem. 563 (2004) 181.
- [13] R.W.J. Scott, A.K. Datye, R.M. Crooks, J. Am. Chem. Soc. 125 (2003) 3708.
- [14] M.-H. Shao, K. Sasaki, R.R. Adzic, J. Am. Chem. Soc. 128 (2006) 3526.
- [15] J. Mathiyarasu, K.L.N. Phani, J. Electrochem. Soc. 154 (2007) B1100.
- [16] C.F. Zinola, J. Rodríguez, J. Solid State Electrochem. 6 (2002) 412.
- [17] M.M.P. Janssen, J. Moolhuysen, Electrochim. Acta 21 (1976) 861.
- [18] B. Bittins-Cattaneo, T. Iwasita, J. Electroanal. Chem. 238 (1987) 151.
- [19] A.S. Arico, V. Antonucci, N. Giordano, A.K. Shukla, M.K. Ravikumar, A. Roy, S.R. Barman, D.D. Sarma, J. Power Sources 50 (1994) 295.
- [20] S. Mukerjee, J. McBreen, J. Electrochem. Soc. 146 (1999) 600.
- [21] G. Stalnionis, L. Tamasauskaitė-Tamasiūnaitė, V. Pautienė, Z. Jusys, J. Solid State Electrochem. 8 (2004) 892.
- [22] A.N. Haner, P.N. Ross, J. Phys. Chem. 95 (1991) 3740.
- [23] P.N. Ross, in: J. Lipkowski, P.N. Ross (Eds.), Electrocatalysis, 1st ed., Wiley-VCH, NY, 1998.
- [24] F. Colmati, E. Antolini, E.R. Gonzalez, Electrochim. Acta 50 (2005) 5496.
- [25] A. Manzo-Robledo, A.-C. Boucher, E. Pastor, N. Alonso-Vante, Fuel Cells 2 (2002) 109.
- [26] B.E. Hayden, M.E. Rendall, O. South, J. Am. Chem. Soc. 125 (2003) 7738.
- [27] A.E. Aksoylu1, M.M.A. Freitas, J.L. Figueiredo, Catal. Today 62 (2000) 337.
- [28] Y. Morimoto, E.B. Yeager, J. Electroanal. Chem. 441 (1998) 77.
- [29] Y. Guo, Y. Zheng, M. Huang, Electrochim. Acta 53 (2008) 3102.
- [30] W. Zhou, Z. Zhou, S. Song, W. Li, G. Sun, P. Tsakaros, Q. Xin, Appl. Catal. B: Environ. 46 (2003) 273.
- [31] F.C. Simões, D.M. dos Anjos, F. Vigier, J.-M. Léger, F. Hahn, C. Coutanceau, E.R. Gonzalez, G. Tremiliosi-Filho, A.R. de Andrade, P. Olivi, K.B. Kokoh, J. Power Sources 167 (2007) 1.
- [32] P. Bommersbach, M. Mohamedi, D. Guay, J. Electrochem. Soc. 154 (2007) B876.
- [33] L. Jiang, Z. Zhou, W. Li, W. Zhou, S.S. Huanqiao Li, G. Sun, Q. Xin, Energy & Fuels 18 (2004) 866.
- [34] F. Coloma, A. Sepúlveda-Escribano, J.L.G. Fierro, F. Rodríguez-Reinoso, Appl. Catal. A: Gen. 136 (1996) 231.
- [35] G. Neri, C. Milone, S. Galvagno, A.P.J. Pijpers, J. Schwank, Appl. Catal. A: Gen. 227 (2002) 105.
- [36] A. Olivas, D.I. Jerdev, B.E. Koel, J. Catal. 222 (2004) 285.

- [37] J.C. Serrano-Ruiz, A. Sepúlveda-Escribano, F. Rodríguez-Reinoso, *J. Catal.* 246 (2007) 158.
- [38] A. Mary Remona, Ph.D. Thesis, Madurai-Kamaraj University, 2006.
- [39] A. Manzo-Robledo, A.-C. Boucher, E. Pastor, N. Alonso-Vante, *Fuel cells* 2 (2002) 109.
- [40] I. Ávila-García, M. Plata-Torres, M.A. Domínguez-Crespo, C. Ramírez-Rodríguez, E.M. Arce-Estrada, *J. Alloys Compd.* 434 (2007) 764.
- [41] H. Yang, C. Coutanceau, J.-M. Leger, N. Alonso-Vante, C. Lamy, *J. Electroanal. Chem.* 576 (2005) 305.
- [42] M.H. Shao, T. Huang, P. Liu, J. Zhang, K. Sasaki, M.B. Vukmirovic, R.R. Adzic, *Langmuir* 22 (2006) 10409.
- [43] A.J. Bard, L.R. Faulkner, *Electrochemical Methods*, 2nd ed., John Wiley & Sons Inc., NY, 2001.
- [44] M.P. Hogarth, G.A. Hards, *Platinum Met. Rev.* 40 (1996) 150.
- [45] A. Heinzel, V.M. Barragan, *J. Power sources* 84 (1999) 70.
- [46] A. Wasmus, A. Kuver, *J. Electroanal. Chem.* 461 (1999) 14.
- [47] R.R. Adzic, in: J. Lipkowski, P.N. Ross (Eds.), *Electrocatalysis*, 1st ed., Wiley-VCH, NY, 1998, p. 210.